Nano Research
2020, 13(9): 2485–2491
Chem.,
ISSN 1998-0124 CN 11-5974/O4
https://doi.org/10.1007/s12274-020-2883-9

Research Article

High-resolution, full-color quantum dot light-emitting diode display fabricated via photolithography approach

Wenhai Mei[1,§], Zhenqi Zhang[1,§], Aidi Zhang[1], Dong Li[1], Xiaoyuan Zhang[1], Haowei Wang[1], Zhuo Chen[1] (✉), Yanzhao Li[1] (✉), Xinguo Li[1,2] (✉), and Xiaoguang Xu[1] (✉)

[1] *BOE Technology Group Co., Ltd., Beijing 100176, China*
[2] *School of Software & Microelectronics Department, Peking University, Beijing 102600, China*
[§] *Wenhai Mei and Zhenqi Zhang contributed equally to this work.*

Received: 3 March 2020 / **Revised:** 15 May 2020 / **Accepted:** 17 May 2020

ABSTRACT

Displays play an extremely important role in modern information society, which creates a never-ending demand for the new and better products and technologies. The latest requirements for novel display technologies focus on high resolution and high color gamut. Among emerging technologies that include organic light-emitting diode (OLED), micro light-emitting diode (micro-LED), quantum dot light-emitting diode (QLED), laser display, holographic display and others, QLED is promising owing to its intrinsic high color gamut and the possibility to achieve high resolution with photolithography approach. However, previously demonstrated photolithography techniques suffer from reduced device performance and color impurities in subpixels from the process. In this study, we demonstrated a sacrificial layer assisted patterning (SLAP) approach, which can be applied in conjunction with photolithography to fabricate high-resolution, full-color quantum dot (QD) patterns. In this approach, the negative photoresist (PR) and sacrificial layer (SL) were utilized to determine the pixels for QD deposition, while at the same time the SL helps protect the QD layer and keep it intact (named PR-SL approach). To prove this method's viability for QLED display manufacture, a 500-ppi, full-color passive matrix (PM)-QLED prototype was fabricated via this process. Results show that there were no color impurities in the subpixels, and the PM-QLED has a high color gamut of 114% National Television Standards Committee (NTSC). To the best of our knowledge, this is the first full-color QLED prototype with such a high resolution. We anticipate that this innovative patterning technique will open a new horizon for future display technologies and may lead to a disruptive and innovative change in display industry.

KEYWORDS

quantum dots, sacrificial layer assisted patterning, quantum dot light-emitting diodes, photolithography, high-resolution

1 Introduction

Beginning from the second half of the 20th century, the information society observed a rapid development from the era of Internet enabled computers, through the era of Mobile Internet on smart phones, to the current era of Internet of Things (IoT) based on smart ports, where high performance displays are to play a key role. To conform to future market trends, display products should meet the demanding requirements in picture quality, power consumption, smart system, fashion, price and environmental friendliness. Resolution, color gamut and size are key attributes to picture quality. To fulfil these requirements and meet the future trends, several emerging technologies are being developed to replace liquid crystal display (LCD), organic light-emitting diode (OLED) [1–3], micro light-emitting diode (micro-LED) [4, 5], quantum dot light-emitting diode (QLED) [6–9], laser display [10, 11], holographic display [12, 13] and others [14, 15].

Among various technologies, OLED has been successfully commercialized and is currently widely utilized as mobile display, resulting into the sales of 470 million AMOLED panels in 2019 [16]; however, it is difficult to reach high resolution (≥ 600 ppi) from evaporation or inkjet printing [17–20]. Micro-LED has extremely high cost due to its insufficient yield of chip transfer and repair; in addition, its efficiency drops significantly when LED chip size getting smaller [4, 5, 21]. Other technologies are mostly in the academic research stage, focusing on working mechanism, efficiency, stability and other primary questions [14, 15].

QLED is another promising technology due to its intrinsic high color gamut owing to quantum dot's narrow emission spectra [22–29]. The external quantum efficiencies (EQEs) of red, green and blue QLEDs have reached up to 24.1%, 22.9%, and 19.8%, respectively [30–32]; while the lifetimes (LT50 @ 100 nits) have reached up to 2,200,000, 1,760,000 and 7,000 h [31, 33]. Another challenge for QLED technology is to form quantum dots (QD) patterns with high resolution without excessive cost [23, 34–40]. Display demos based on various approaches have been developed for QLED's commercialization. In 2011, Samsung fabricated a 4-inch demo with a resolution of 100 ppi, that was formed by transfer printing [38]. BOE demonstrated 5- and 14-inch inkjet-printed prototypes with a

Address correspondence to Zhuo Chen, chenzhuo_cto@boe.com.cn; Yanzhao Li, liyanzhao@boe.com.cn; Xinguo Li, lixinguo@boe.com.cn; Xiaoguang Xu, xuxiaoguang@boe.com.cn

resolution of 80 ppi in 2017 [41]. However, neither of the process can meet all the requirements including high resolution, large area production and low cost. A practical patterning approach that would meet the above requirements can be a photolithography process [42–48]. The photolithography approach has achieved high-resolution and full-color patterning of single layer of QDs, especially for photoluminescent (PL) applications; however, no high-resolution full-color electroluminescent (EL) QD display prototype has been reported. The requirements for QD patterning in EL applications are much stricter than in PL applications. Firstly, the emission of unwanted QD residues (e.g., red QDs in green subpixels, if not removed completely) can be noticeable in EL applications and cause color impurities in full-color QLED device and lower the color gamut of the display. Secondly, an EL device is very sensitive to the material purities of each layer; if the patterned QD layer is contaminated, dissolved or damaged by the photolithography process, the efficiency and lifetime of the EL device will be degraded. In order to realize a full-color QLED device, the issues of color impurities and device performance degradation shall be addressed.

Two main photolithography approaches to pattern QDs have been developed. One is to chemically modify the ligands of QDs or add photoactive additives in QDs to make the QD layer photoactive and photo-patternable [49–52]. A major issue of this approach is that the unwanted QD residues are difficult to be removed completely during development, leading to color impurities. The other approach is to utilize photoresists (PRs) and conventional photolithography to define the subpixels for QD deposition [53–55]. In this approach the QDs in "unwanted" subpixels would be deposited on top of the PR layer and will be removed along PR in the lift-off process. This approach avoids color impurity problem, but may cause other critical issues. Firstly, the chemicals used in the conventional photolithography and lift-off process (solvent of PR, developer, and stripper) may contaminate, dissolve or damage the pre-existing QD patterns, leading to trap sites formation and increased luminescence quenching in the electroluminescent devices. Secondly, the PR may not be removed completely during lift-off process and the PR residues would affect the device performance.

The two approaches discussed above can be classified as direct approach, as the pixelated patterns are directly formed by the photolithography process. The problems to fabricate full-color QLED display mainly come from the QD/substrate or QD/PR interfaces in direct approaches. It is difficult to meet the requirements of both interfaces intact and photo-patternable with the same materials. In order to address the issues in a full color QLED display, we proposed an indirect approach, which is called "sacrificial layer assisted patterning" (SLAP). In the SLAP approach, the pixelated patterns are transferred to another layer (sacrificial layer (SL)), and then transferred from SL to QD layers. Then interfacial and patternable requirements can be fulfilled by two materials. The issues that are present at the QD/substrate or QD/PR interfaces during the direct approach are now lying on the PR/SL interface, which can be eliminated if the SL materials are properly chosen. The SL materials are not necessary to be photo-responsive, but instead this technology can be combined with various patterning technologies, such as photolithography, transfer printing, laser direct writing, and so on, to achieve easy QD patterning. Thus the SLAP concept has a wide range of application.

In this study, we present the process in which the SLAP approach is applied in conjunction with photolithography. The negative PR and SL were utilized to determine the pixels for QD deposition, while at the same time the SL helps to protect the QD layer and keep it intact. With this PR-SL approach, we prepared a 500-ppi full-color passive matrix (PM)-QLED device (subpixel size of 5 μm × 39 μm) without color impurities in subpixels. To the best of our knowledge, it is the first full color QLED display prototype achieving 500 ppi. This process demonstrates the possibility of achieving high-performance, high-resolution display with traditional instruments and process in backplane manufacture; it would lead to a disruptive and innovative change in display industry.

2 Results and discussion

2.1 Patterning of QDs

As discussed in the previous section, in order to realize a full-color QLED device, a PR-SL approach is proposed, in which the SL is utilized to transfer the pixelated patterns to the QD layer, and to protect QD layer in the photolithography process. In this approach, the design or the selection of the SL materials is critical. The SL should meet the following criteria. Firstly, the solvent of the sacrificial material shall be orthogonal to QDs, so the deposition of SL would not dissolve or damage the QD layer. Secondly, it shall have good film-forming property to fully cover the QD layers and it shall not interact with the solvent and developer of PRs, thus the SL is able to protect the QD layers during the successive patterning. Thirdly, the SL shall have a low adhesion to QD layer, and have a high solubility in its solvent, so the SL can be readily removed without residues in mild conditions. Fourthly, the PR shall be able to form a stable pattern on the SL.

According to the criteria, polyvinylpyrrolidone (PVP) is chosen as the sacrificial material. PVP is highly soluble in ethanol, which is known to be orthogonal to the commercially available quantum dots with alkyl thiol ligands. At the same time, due to its polar structure, PVP has low adhesion to QD layers with non-polar ligands, so PVP can be removed readily without residues in mild conditions. Again, due to its polarity, the SL won't be swelled or dissolved by the non-polar solvent and developer of PR (xylene in this study), preventing the chemicals to penetrate the SL and touch the QD layer. In addition, the negative PR can be well-patterned on PVP layer based on our results.

As Fig. 1 illustrates, red, green and blue QDs are patterned in sequence. A 0.5 mm thick glass is used as the patterning substrate. A SL, which is composed of PVP, is spin-coated onto the substrate (step 1). The SL can be easily dissolved in alcohols helping to lift-off the PRs. Then, a negative PR is coated onto the SL and exposed to a UV light of 365 nm through a mask (step 2 and 3). The "unwanted" subpixels are exposed so that the negative PR will remain on the substrate, while the PRs on the wanted subpixels are washed away during developing, leaving the SL materials exposed. Then, the substrate is dry-etched via inductively coupled plasma (ICP) etching (step 4). Thus, the glass substrates are exposed in the wanted subpixels, while the unwanted subpixels are covered by SL and PR.

After that, the red QDs with alkyl thiol ligands are spin-coated onto the substrate (step 5). The thickness of the red QDs can be controlled by the concentrations and spin rates. After QD deposition, the PR patterned substrate is immersed in alcohols in ultrasonic bath to lift-off the SL (step 6), PR and the QDs coated on top of the PR (leading to complete removal of QDs in unwanted subpixels), providing the first QD patterns (red QDs) on the glass substrate. The SL deposition, PR patterning, ICP etching, QD coating and lift-off process

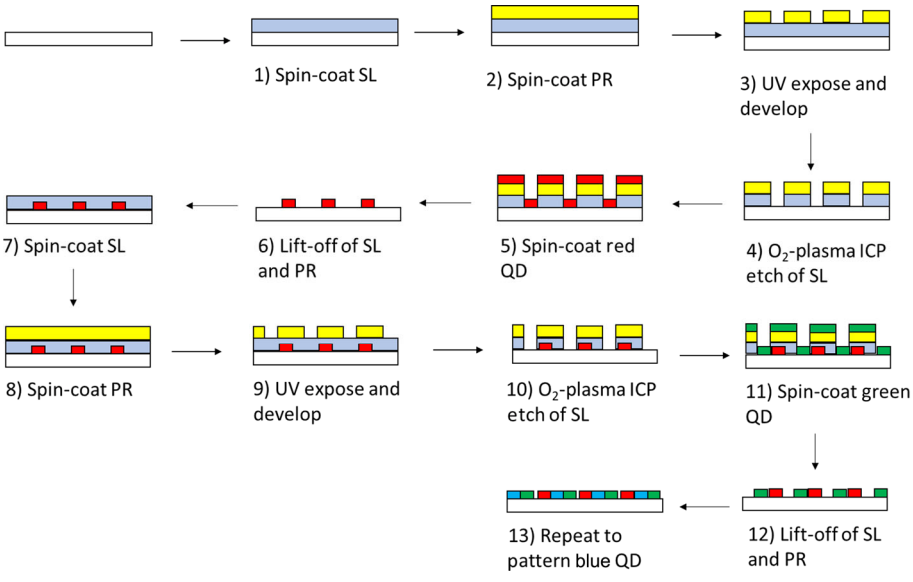

Figure 1 Schematic illustration of patterning QDs with different color on a substrate via photolithography approach.

(step 1 to 6) compose a cycle of one-color QD patterning. The cycle can be repeated for green and blue QDs patterning.

The key consideration in the process is to keep the QD layer intact. The QDs used in this study are CdSe/ZnS QDs with alkyl thiol ligands, which is widely used in QLED device. The SL material (PVP) is highly soluble in alcohols. Thus, the solvent chosen for the SL coating (step 1 and 7) and ultrasonic lift-off (step 6 and 12) is ethanol, in which the QDs are insoluble. In addition, the ultrasonication lift-off of PVP is very quick in ethanol, leading to minimal possible damage to QD patterns during lift-off. During PR deposition in the repeated process, the pre-patterned QDs are protected by SL to avoid contacting with PR and PR solvents. In addition, the pre-patterned QDs are protected by SL and PR during the ICP etching. In other words, the pre-patterned QDs are kept intact due to the combination of SL and PR layers.

The size of QD patterns is determined by mask used during PR exposure. In this study, the QD pattern with a 5 μm × 39 μm size was achieved. Figure 2 demonstrates the photoluminescence image of the patterned R/G/B QDs on a glass substrate with 405 nm ultraviolet excitation. The luminance of red was suppressed to 10% by the microscope software to clearly show the green and blue patterns. The merits of this process are well supported by the fact that the size of the emitting area matches very well with that of a pristine pixel and all the pixels exhibit clear patterns. The PL image shows uniform brightness in each pixel and no color impurities are observed. These results indicate the validity of the photolithography approach to pattern multi-color QDs and motivate us to apply this approach to electroluminescence devices.

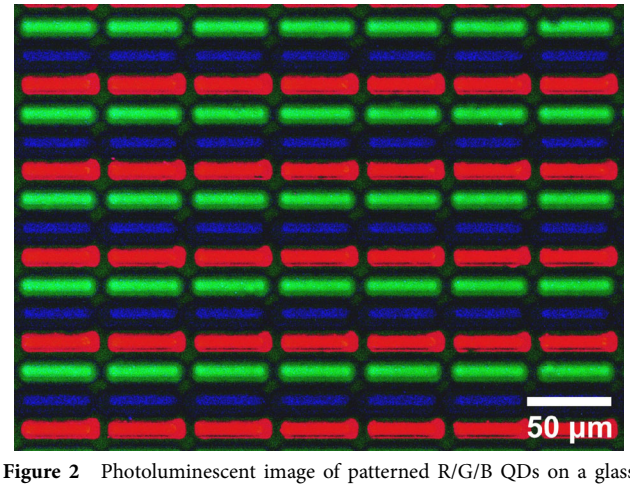

Figure 2 Photoluminescent image of patterned R/G/B QDs on a glass substrate with 405 nm ultraviolet excitation. The brightness of red was suppressed to 10% by the microscope software to clearly show the green and blue patterns.

2.2 QLED device performance

Considering the stability requirements for the underlayer on which the QDs are patterned, we chose to utilize inverted QLED structure to verify the photolithography approach, as shown in Fig. 3(a); the device architecture used in this study is ITO/ZnO nanoparticles/QDs/HT-1/HT-2/HAT-CN/Ag. Indium tin oxide (ITO) was used as a cathode. Zinc oxide (ZnO) nanoparticles were spin-coated as an electron-transporting layer (ETL). As ZnO nanoparticles have short ligands of ethanolamine, the ZnO nanoparticles film is relatively stable and resisting to alcohols that will be used in the patterning process. Two hole-transporting (HT) materials were used in this study. HT-1 has deeper highest occupied molecular orbitals (HOMO, −5.7 eV) but lower hole mobility (~ 10^{-6} $cm^2 \cdot V \cdot s^{-1}$), while HT-2 has higher hole mobility (~ 10^{-4} $cm^2 \cdot V \cdot s^{-1}$) but shallower HOMO (−5.5 eV). A thin layer of HT-1 was inserted between QD and HT-2 to improve hole injection. 1, 4, 5, 8, 9, 11-Hexaazatriphenylenehexacarbonitrile (HAT-CN) was used as the hole-injection (HI) materials and silver (Ag) film acted as the anode. The energy level diagram of each layer is depicted in Fig. 3(b), and theoretically explains the practicality of the device structure.

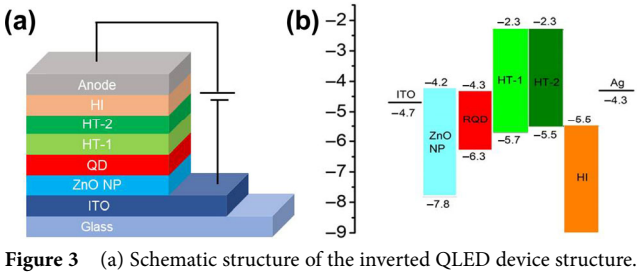

Figure 3 (a) Schematic structure of the inverted QLED device structure. (b) The energy diagram of the inverted QLED device (take red device as an example).

For proof-of-concept purpose, we investigated the effect of patterning process on the efficiency of single-color device. We simulated the whole patterning process except coating different QDs (patterned devices). ZnO nanoparticles were spin-coated onto the patterned ITO with pixel size of 2 mm × 2 mm. Then PVP was used as the SL and spin-coated onto ZnO layer using an ethanol solution. The substrate was then coated with negative PR and developed in p-xylene (without exposure). After that oxygen-plasma ICP was utilized to etch the SL layer, leaving ZnO layer exposed. QDs were deposited onto ZnO layer and then the device was immersed into alcohols and ultrasonicated (to simulate lift-off of PR and SL). Then the sample was transferred to a vacuum deposition chamber where HT, HI and Ag anode were sequentially deposited via thermal evaporation. The devices were encapsulated with a UV-curable epoxy and cover glass in the N_2 atmosphere. The detailed process is demonstrated in Fig. S1 in the Electronic Supplementary Material (ESM).

The comparison of electroluminescence performance between these control devices (R/G/B single-color devices without any patterning processes) and patterned devices are summarized in Fig. 4. The current density-voltage and luminance-voltage characteristics are shown in Figs. 4(a) and 4(b), respectively. We can see clearly that the current density and luminance of red and green devices showed a slight increase after the patterned process, which may be caused by the QD film thickness decrease during the ultrasonic process. Figure 4(c) shows that, after the patterning process, the red and green patterned devices exhibited no obvious decrease compared with their corresponding control devices. The current efficiencies decreased slightly from 12.8 to 10.4 cd·A^{-1} for red, from 29.8 to 25.4 cd·A^{-1} for green, indicating that the performance of the red and green devices is preserved after the pattering process.

The performance of the blue patterned device was found to significantly degrade after the PR-SL process. The voltage at which luminance reaches 100 nits decreased from 8.4 to 4.2 V, while the current density noticeably increased, with the current efficiency reducing from 1.1 to 0.4 cd·A^{-1}. The mechanism for the device performance degradation is not quite clear yet, but in our opinion, there are three possible reasons for it. Firstly, the oxygen vacancies of ZnO might have been affected by plasma treatment, resulting into reduced number of the surface trap sites and as a result a trap-filled current onset at a lower voltage [56–58]. Secondly, the blue QDs may be more impacted by the patterning process, because of the relatively high level of core-shell lattice mismatch due to a smaller core size. Comparing to the green and red QDs, the shell of the blue QDs has more defects, which is more susceptible to the patterning process. It is therefore possible that a large number of mid-gap states were formed, providing an easier charge injection, but not contributing to radiative recombination [59–61]. Thus the leakage current increases, leading to the current efficiency drop. Thirdly, after the patterning process, the photoluminescent quantum yield (PLQY) of QD films decrease from 58%, 55% and 39% to 51%, 47% and 29% for red, green and blue devices, respectively (Fig. S2 in the ESM). The blue QD film exhibits a larger PLQY decrease than red and green films during the patterning process, which might also play a role in the current efficiency being affected stronger compared to the red and green QDs. The detailed mechanism for the blue device performance change is still under investigation in our group. However, the performance of red and green devices after the lithography process has demonstrated the viability of the PR-SL approach.

The EL spectra for each emission color are shown in Fig. 4(d). The R/G/B control devices exhibit emission peaks at 628, 527 and 468 nm, and very narrow emission spectrum with full width at half-maximum (FWHM) of 28, 25 and 28 nm, respectively. After the patterning process, we observed just small changes in the green patterned devices, with the emission peak at 524 nm and FWHM of 23 nm. In summary, the performance of devices preserved after the process, which encourages the fabrication of a full-color device.

2.3 Full-color PM-QLED device performance

To confirm the feasibility of the photolithographic patterning process in preparing the high-resolution QLED displays, a 500-ppi full-color PM-QLED device was fabricated. The device was fabricated on a passive matrix substrate, with the subpixel size of 5 μm × 39 μm. The device structure and

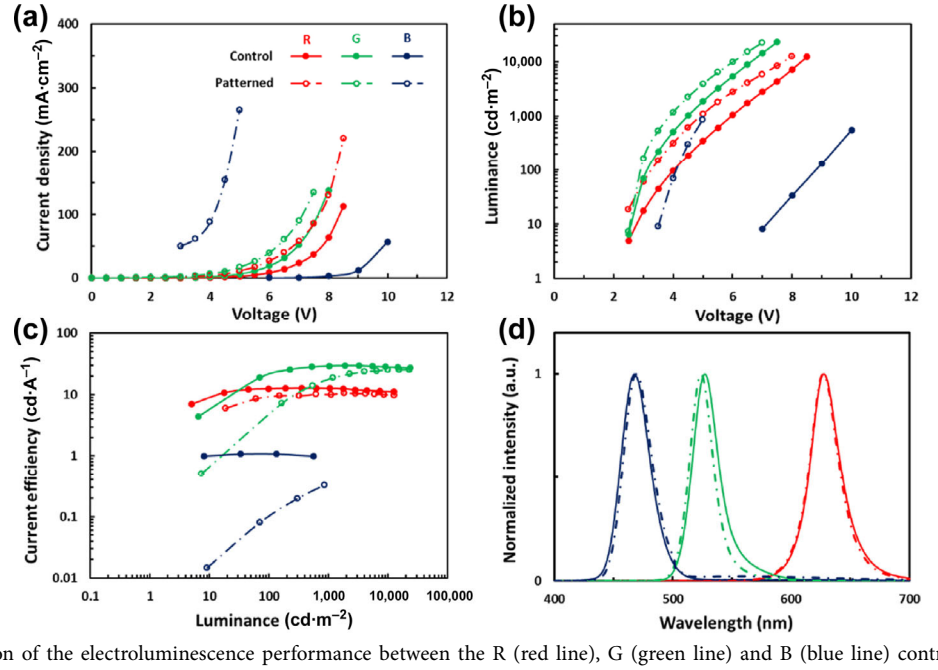

Figure 4 Comparison of the electroluminescence performance between the R (red line), G (green line) and B (blue line) control (straight line) and patterned (dash line) devices. (a) Current density–voltage characteristics. (b) Luminance–voltage characteristics. (c) Current efficiency. (d) EL emission spectra.

fabrication are the same as the control and patterned devices discussed in the previous section, except red, green and blue QDs were consequently patterned with the photolithography approach, as illustrated in Fig. 1.

Figure 5(a) shows the simultaneous R/G/B electroluminescence from the pixels. The red, green and blue subpixels can also be lit separately (Fig. 5(b) inserts). The EL spectra of each color emission are shown in Fig. 5(b), in which the R, G, B subpixels show unimodal emission peaks at 628, 525 and 465 nm, without color impurities in the subpixels. These results indicate that our novel QD patterning technique can efficiently avoid the color impurities in subpixels. The CIE 1931 chromaticity coordinates of each color are shown as (0.69, 0.31), (0.16, 0.77), and (0.15, 0.07) for red, green and blue in Fig. 5(c), leading to a color gamut of 114% NTSC for the PM-QLED device. To the best of our knowledge, this PM-QLED display is the first full-color QLED prototype with a high resolution of up to 500 ppi. The current efficiencies of the PM-QLED are measured as 8.3 cd·A^{-1} for red, 9.8 cd·A^{-1} for green and 0.02 cd·A^{-1} for blue, while the maximum luminescence reaches 108,000 nits for red, 247,000 nits for green, and 340 nits for blue, respectively. The efficiency drops may come from the small pixel size, but the detailed mechanism is still under investigation. We are currently working on the optimizing processing conditions to improve the device efficiencies.

3 Conclusions

In conclusion, we presented a novel indirect SLAP approach to achieve a high-resolution full-color QLED display. In conjunction with photolithography, we demonstrated a PR-SL process, in which the negative photoresist and SL were utilized to determine the pixels for QD deposition, while at the same time the SL helps to avoid the interfacial issues in the devices. The performance of the patterned QLED devices after the process shows no obvious decline from the control devices, indicating that this method is effective to construct patterned QDs without observable damage. The resolution of QD patterns was determined by the exposure mask and by the optical limitation of photolithography process. As a result, a 500-ppi, full-color PM-QLED display prototype was fabricated via this approach. The PM-QLED showed unimodal emission from each subpixel without color impurities, leading to the color gamut over 114% NTSC. To the best of our knowledge, it is the first reported full-color QLED display with the resolution as high as 500 ppi. The PR-SL approach can be adopted utilizing photolithography instrumentations from the current array and color filter production process without extra investments. This method eliminates big obstacles and firstly verifies the possibility for mass production of high-resolution QLED. It may be applied to the mass-production of large-size high-resolution QLED displays that meet the requirements for future market. And this photolithography process is capable of providing next generation displays with higher qualities at the reduced costs.

4 Method

4.1 Materials

The QDs for red, green and blue were cadmium selenide core/shell colloidal dots purchased from Suzhou Xingshuo Nanotech Co., Ltd. Zinc oxide nanoparticles solution (ZnO NPs) were manufactured by Poly OptoElectronics Tech. Ltd.. Polyvinyl pyrrolidone K30 (PVP K30) resins were obtained from Gobekie Ltd.. Photoresist (BN308-150) was obtained from Kempur Microelectronics Inc. HT-1 and HT-2 materials are not disclosed for reasons of confidentiality. 1,4,5,8,9,11-Hexaazatriphenylenehexacarbonitrile (HAT-CN) was purchased from J&K Scientific. Silver (99.99%) evaporation material was bought from CNM Inc.. Other solvents used were all super dry grade obtained from Shanghai Titan Tech. Ltd..

4.2 Control QLED device fabrication

The control QLED devices were fabricated through spin-coating and evaporation on glass substrates with pre-patterned ITO cathode. The pixel size is 2 mm × 2 mm. First, the substrates were carefully cleaned in deionized water, acetone, and ethyl alcohol for 15 min each. Then the substrates were treated with UV-ozone for 10 min for removal of organic residue on the surface. After that the substrates were annealed for 5 min at 120 °C in the glovebox. ZnO NPs were spin-coated onto the substrate at 1,500 rpm for 40 s using a 30 mg·mL^{-1} solution in ethanol and annealed at 120 °C for 20 min. The QDs were spin-coated at 2,500 rpm and annealed at 120 °C for 20 min. When the QD layer was finished, the samples were transferred to a vacuum deposition chamber with chamber pressure below 5 × 10^{-6} torr for HT, HI and Ag anode deposition. The devices were capsulated with a UV-curable epoxy and cover glasses in the N_2 atmosphere. The QLED devices utilize the architecture ITO/ZnO/QD/HT-1/HT-2/HI/Ag.

4.3 Patterned QLED device fabrication

The patterned substrates were treated according to the same method as control ones. ZnO NPs were spin-coated onto the substrate (with a pixel size of 2 mm × 2 mm) and annealed on a hot plate at 120 °C for 20 min. The PVP K-30 was chosen as the SL and spin-coated at 1,500 rpm using a 30 mg·mL^{-1} solution in ethanol. Then the substrates were deposited with PR at 4,000 rpm and developed in the p-xylene for 90 s (without exposure). ICP was employed to etch the sacrificial layer. The QDs were spin-coated at 2,500 rpm and the

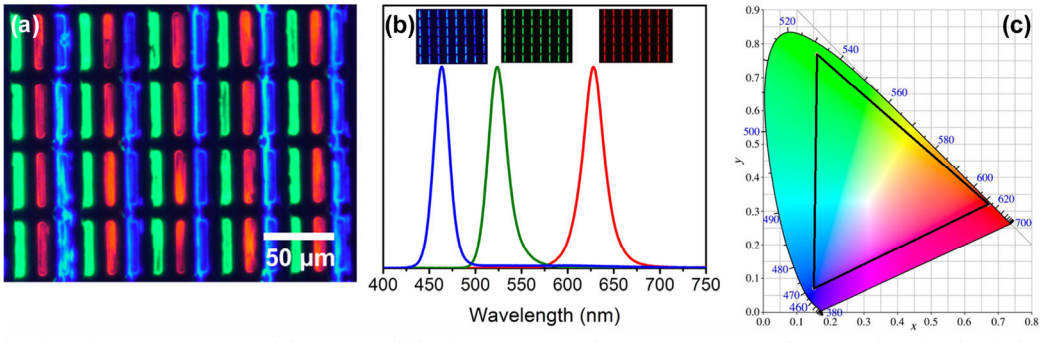

Figure 5 (a) The electroluminescent image of the 500-ppi, full-color PM-QLED. (b) Emission spectra of R/G/B subpixels when lightening separately. (c) Color coordinates of R/G/B subpixels when lightening separately.

substrates were rinsed in the ethanol for 4 min by sonication. Next, the films were annealed at 120 °C for 20 min. When the QD layer was finished, the samples were transferred to a vacuum deposition chamber with chamber pressure below 5×10^{-6} torr for HT, HI and Ag anode deposition. The devices were capsulated with a UV-curable epoxy and cover glasses in the N_2 atmosphere.

4.4 Full-color PM-QLED device fabrication

Firstly, the PM substrates were carefully treated according to the same method as control ones. Then ZnO NPs were spin-coated onto the substrate and baked at 120 °C for 20 min. The PVP K-30 was chosen as the SL and spin-coated at 1,500 rpm using a 30 mg·mL^{-1} solution in ethanol. Then the substrates were deposited with PR at 4,000 rpm and exposed for 3 s following (365 nm, 18 mJ·cm^{-2}). After the exposure, the substrates were developed in the p-xylene for 90 s to form the PR patterns. ICP was employed to etch the uncovered SL, which was not protected by the PR after the developing. The QDs were spin-coated at 2,500 rpm and the substrates were rinsed in the ethanol for 4 min by ultrasonic. At last, the membranes were annealed at 120 °C for 20 min. The green and blue QD membranes were patterned by repeating above processes. When all the QD layers were finished, the samples were transferred to a vacuum deposition chamber with chamber pressure below 5×10^{-6} torr for HT, HI and Ag anode deposition. The devices were capsulated with a UV-curable epoxy and cover glasses in the N_2 atmosphere.

4.5 Characterization

The current-voltage-luminance (*I*–*V*–*L*) characteristics of the devices were measured by a Keithley-2400 source unit coupled with a calibrated CS-1000 CCD camera. The QLED lifetimes were characterized by Chroma Model 58131 OLED lifetime test system.

The PLQYs of quantum dots were measured by the Hamamatsu C9920-11 absolute PL quantum yield spectrometer. The photoluminescence images were obtained with an Olympus IX73 fluorescence microscope. The electroluminescent images were obtained by a Nikon LV100 ND optical microscope.

Acknowledgements

This work was supported by the National Key R&D Program of China (No. 2016YFB0401700).

Electronic Supplementary Material: Supplementary material (including the process of fabricating proof-of-concept patterned device, the lifetime data and PLQY data) is available in the online version of this article at https://doi.org/10.1007/s12274-020-2883-9.

References

[1] Salehi, A.; Fu, X. Y.; Shin, D. H.; So, F. Recent advances in OLED optical design. *Adv. Funct. Mater.* **2019**, *29*, 1808803.

[2] Wei, Q.; Fei, N. N.; Islam, A.; Lei, T.; Hong, L.; Peng, R. X.; Fan, X.; Chen, L.; Gao, P. Q.; Ge, Z. Y. Small-molecule emitters with high quantum efficiency: Mechanisms, structures, and applications in OLED devices. *Adv. Opt. Mater.* **2018**, *6*, 1800512.

[3] Wong, W. Y.; Ho, C. L. Functional metallophosphors for effective charge carrier injection/transport: New robust OLED materials with emerging applications. *J. Mater. Chem.* **2009**, *19*, 4457–4482.

[4] Wu, T. Z.; Sher, C. W.; Lin, Y.; Lee, C. F.; Liang, S. J.; Lu, Y. J.; Huang Chen, S. W.; Guo, W. J.; Kuo, H. C.; Chen, Z. Mini-LED and micro-LED: Promising candidates for the next generation display technology. *Appl. Sci.* **2018**, *8*, 1557.

[5] Huang, Y. G.; Tan, G. J.; Gou, F. W.; Li, M. C.; Lee, S. L.; Wu, S. T. Prospects and challenges of mini-LED and micro-LED displays. *J. Soc. Inf. Disp.* **2019**, *27*, 387–401.

[6] Rogach, A. L.; Gaponik, N.; Lupton, J. M.; Bertoni, C.; Gallardo, D. E.; Dunn, S.; Li Pira, N.; Paderi, M.; Repetto, P.; Romanov, S. G. et al. Light-emitting diodes with semiconductor nanocrystals. *Angew. Chem., Int. Ed.* **2008**, *47*, 6538–6549.

[7] Pietryga, J. M.; Park, Y. S.; Lim, J.; Fidler, A. F.; Bae, W. K.; Brovelli, S.; Klimov, V. I. Spectroscopic and device aspects of nanocrystal quantum dots. *Chem. Rev.* **2016**, *116*, 10513–10622.

[8] Erdem, T.; Demir, H. V. Color science of nanocrystal quantum dots for lighting and displays. *Nanophotonics* **2013**, *2*, 57–81.

[9] Shirasaki, Y.; Supran, G. J.; Bawendi, M. G.; Bulović, V. Emergence of colloidal quantum-dot light-emitting technologies. *Nat. Photonics* **2013**, *7*, 13–23.

[10] Yuan, Y.; Bi, Y.; Sun, M. Y.; Wang, D. Z.; Wang, D. D.; Gao, W. N.; Zhang, S. Speckle evaluation in laser display: From speckle contrast to speckle influence degree. *Opt. Commun.* **2020**, *454*, 124405.

[11] Hargis, D. E.; Takeuchi, E. B.; Bergstedt, R.; Flint, G.; Nelte, S.; Pessot, M. Solid-state laser-based displays. *SID Symp. Dig. Tech. Pap.* **1999**, *30*, 986–989.

[12] Yaraş, F.; Kang, H.; Onural, L. Circular holographic video display system. *Opt. Express* **2011**, *19*, 9147–9156.

[13] Khan, J.; Blackwell, C.; Can, C.; Underwood, I. 16-1: *Invited Paper*: Holographic volumetric 3D displays. *SID Symp. Dig. Tech. Pap.* **2018**, *49*, 177–180.

[14] Zhang, L. Q.; Yang, X. L.; Jiang, Q.; Wang, P. Y.; Yin, Z. G.; Zhang, X. W.; Tan, H. R.; Yang, Y.; Wei, M. Y.; Sutherland, B. R. et al. Ultra-bright and highly efficient inorganic based perovskite light-emitting diodes. *Nat. Commun.* **2017**, *8*, 15640.

[15] Xiao, Z. G.; Kerner, R. A.; Zhao, L. F.; Tran, N. L.; Lee, K. M.; Koh, T. W.; Scholes, G. D.; Rand, B. P. Efficient perovskite light-emitting diodes featuring nanometre-sized crystallites. *Nat. Photonics* **2017**, *11*, 108–115.

[16] Summary of the global AMOLED smartphone panel market in 2019. *Sigmaintell* **2020**. http://www.sigmaintell.com/en/search.php?cid=41&keys=Summary+of+the+global+AMOLED+smartphone+panel+market+in+2019.

[17] Ando, M.; Imai, T.; Yasumatsu, R.; Matsumi, T.; Tanaka, M.; Hirano, T.; Sasaoka, T. 68.3: WITHDRAWN 68.4L: *Late-News Paper*: High-resolution printing of OLED displays. *SID Symp. Dig. Tech. Pap.* **2012**, *43*, 929–932.

[18] Gensler, M.; Boeffel, C.; Kröpke, S.; Kronemeijer, A. J.; Ke, T. H.; Papadopoulos, N.; Yao, J.; Stark, J.; Obene, P. 82 - 5: *Late-News Paper*: High-resolution printing for future processing of RGB OLED displays. *SID Symp. Dig. Tech. Pap.* **2018**, *49*, 1117–1119.

[19] Lee, M. T.; Shen, S. M.; Weng, Z. X.; Fu, J. J.; Chen, C. L.; Chuang, C. S.; Lin, Y. 40.3: One FMM solution for achieving active-matrix OLED with 413 ppi real pixel density. *SID Symp. Dig. Tech. Pap.* **2014**, *45*, 573–575.

[20] Lih, J. J.; Chao, C. I.; Lee, C. C. 40.4: *Invited Paper*: The challenge of high resolution to active-matrix OLED. *SID Symp. Dig. Tech. Pap.* **2006**, *37*, 1459–1462.

[21] Jeon, C. W.; Kim, K. S.; Dawson, M. D. Fabrication of two-dimensional InGaN-based micro-LED arrays. *Phys. Status Solidi (A)* **2002**, *192*, 325–328.

[22] Li, D.; Kristal, B.; Wang, Y. J.; Feng, J. W.; Lu, Z. G.; Yu, G.; Chen, Z.; Li, Y. Z.; Li, X. G.; Xu, X. G. Enhanced efficiency of InP-based red quantum dot light-emitting diodes. *ACS Appl. Mater. Interfaces* **2019**, *11*, 34067–34075.

[23] Sabeeh, A.; Thakur, Y.; Ruzyllo, J. Lift-off patterning of nano-crystalline quantum dot films. *ECS Trans.* **2015**, *69*, 53–57.

[24] Li, Y.; Hou, X. Q.; Dai, X. L.; Yao, Z. L.; Lv, L. L.; Jin, Y. Z.; Peng, X. G. Stoichiometry-controlled InP-based quantum dots: Synthesis, photoluminescence, and electroluminescence. *J. Am. Chem. Soc.* **2019**, *141*, 6448–6452.

[25] Coe, S.; Woo, W. K.; Bawendi, M.; Bulović, V. Electroluminescence from single monolayers of nanocrystals in molecular organic devices. *Nature* **2002**, *420*, 800–803.

[26] Colvin, V. L.; Schlamp, M. C.; Alivisatos, A. P. Light-emitting diodes made from cadmium selenide nanocrystals and a semiconducting polymer. *Nature* **1994**, *370*, 354–357.

[27] Dai, X. L.; Zhang, Z. X.; Jin, Y. Z.; Niu, Y.; Cao, H. J.; Liang, X. Y.; Chen, L. W.; Wang, J. P.; Peng, X. G. Solution-processed, high-performance light-emitting diodes based on quantum dots. *Nature* **2014**, *515*, 96–99.
[28] Won, Y. H.; Cho, O.; Kim, T.; Chung, D. Y.; Kim, T.; Chung, H.; Jang, H.; Lee, J.; Kim, D.; Jang, E. Highly efficient and stable InP/ZnSe/ZnS quantum dot light-emitting diodes. *Nature* **2019**, *575*, 634–638.
[29] Mashford, B. S.; Stevenson, M.; Popovic, Z.; Hamilton, C.; Zhou, Z. Q.; Breen, C.; Steckel, J.; Bulovic, V.; Bawendi, M.; Coe-Sullivan, S. et al. High-efficiency quantum-dot light-emitting devices with enhanced charge injection. *Nat. Photonics* **2013**, *7*, 407–412.
[30] Ding, K.; Fang, Y. S.; Dong, S. H.; Chen, H. T.; Luo, B. B.; Jiang, K.; Gu, H. G.; Fan, L. W.; Liu, S. Y.; Hu, B. et al. 24.1% external quantum efficiency of flexible quantum dot light-emitting diodes by light extraction of silver nanowire transparent electrodes. *Adv. Opt. Mater.* **2018**, *6*, 1800347.
[31] Shen, H. B.; Gao, Q.; Zhang, Y. B.; Lin, Y.; Lin, Q. L.; Li, Z. H.; Chen, L.; Zeng, Z. P.; Li, X. G.; Jia, Y. et al. Visible quantum dot light-emitting diodes with simultaneous high brightness and efficiency. *Nat. Photonics* **2019**, *13*, 192–197.
[32] Wang, L. S.; Lin, J.; Hu, Y. S.; Guo, X. Y.; Lv, Y.; Tang, Z. B.; Zhao, J. L.; Fan, Y.; Zhang, N.; Wang, Y. J. et al. Blue quantum dot light-emitting diodes with high electroluminescent efficiency. *ACS Appl. Mater. Interfaces* **2017**, *9*, 38755–38760.
[33] Cao, W. R.; Xiang, C. Y.; Yang, Y. X.; Chen, Q.; Chen, L. W.; Yan, X. L.; Qian, L. Highly stable QLEDs with improved hole injection via quantum dot structure tailoring. *Nat. Commun.* **2018**, *9*, 2608.
[34] Kim, B. H.; Onses, M. S.; Lim, J. B.; Nam, S.; Oh, N.; Kim, H.; Yu, K. J.; Lee, J. W.; Kim, J. H.; Kang, S. K. et al. High-resolution patterns of quantum dots formed by electrohydrodynamic jet printing for light-emitting diodes. *Nano Lett.* **2015**, *15*, 969–973.
[35] Jiang, C. B.; Mu, L.; Zou, J. H.; He, Z. W.; Zhong, Z. J.; Wang, L.; Xu, M.; Wang, J.; Peng, J. B.; Cao, Y. Full-color quantum dots active matrix display fabricated by ink-jet printing. *Sci. China Chem.* **2017**, *60*, 1349–1355.
[36] Jiang, C. B.; Zhong, Z. M.; Liu, B. Q.; He, Z. W.; Zou, J. H.; Wang, L.; Wang, J.; Peng, J. B.; Cao, Y. Coffee-ring-free quantum dot thin film using inkjet printing from a mixed-solvent system on modified ZnO transport layer for light-emitting devices. *ACS Appl. Mater. Interfaces* **2016**, *8*, 26162–26168.
[37] Kim, L.; Anikeeva, P. O.; Coe-Sullivan, S. A.; Steckel, J. S.; Bawendi, M. G.; Bulović, V. Contact printing of quantum dot light-emitting devices. *Nano Lett.* **2008**, *8*, 4513–4517.
[38] Kim, T. H.; Cho, K. S.; Lee, E. K.; Lee, S. J.; Chae, J.; Kim, J. W.; Kim, D. H.; Kwon, J. Y.; Amaratunga, G.; Lee, S. Y. et al. Full-colour quantum dot displays fabricated by transfer printing. *Nat. Photonics* **2011**, *5*, 176–182.
[39] Choi, M. K.; Yang, J.; Kang, K.; Kim, D. C.; Choi, C.; Park, C.; Kim, S. J.; Chae, S. I.; Kim, T. H.; Kim, J. H. et al. Wearable red-green-blue quantum dot light-emitting diode array using high-resolution intaglio transfer printing. *Nat. Commun.* **2015**, *6*, 7149.
[40] Kim, B. H.; Nam, S.; Oh, N.; Cho, S. Y.; Yu, K. J.; Lee, C. H.; Zhang, J. Q.; Deshpande, K.; Trefonas, P.; Kim, J. H. et al. Multilayer transfer printing for pixelated, multicolor quantum dot light-emitting diodes. *ACS Nano* **2016**, *10*, 4920–4925.
[41] Li, Y. Z.; Chen, Z.; Kristal, B.; Zhang, Y. M.; Li, D.; Yu, G.; Wang, X. Y.; Wang, L.; Shi, Y. M.; Wang, Z. L. et al. 80 - 1: *Invited Paper*: Developing AMQLED technology for display applications. *SID Symp. Dig. Tech. Pap.* **2018**, *49*, 1076–1079.
[42] Pickering, S.; Kshirsagar, A.; Ruzyllo, J.; Xu, J. Patterned mist deposition of tri-colour CdSe/ZnS quantum dot films toward RGB LED devices. *Opto-Electron. Rev.* **2012**, *20*, 148–152.
[43] Wang, J.; Wang, C. F.; Shen, H. X.; Chen, S. Quantum-dot-embedded ionomer-derived films with ordered honeycomb structures via breath figures. *Chem. Commun.* **2010**, *46*, 7376–7378.
[44] Kwon, J. H.; Ji, S. H.; Han, S. H.; Kwak, M. S.; Jun, M.; Kang, I. B. P-184: Improvement of color mixing in high PPI mobile displays. *SID Symp. Dig. Tech. Pap.* **2016**, *47*, 1830–1833.
[45] Oh, S. D.; Kim, J.; Lee, D. H.; Kim, J. H.; Jang, C. W.; Kim, S.; Choi, S. H. Structural and optical characteristics of graphene quantum dots size-controlled and well-aligned on a large scale by polystyrene-nanosphere lithography. *J. Phys. D. Appl. Phys.* **2015**, *49*, 025308.
[46] Hayashi, T.; Shibata, T.; Kawashima, T.; Makino, E.; Mineta, T.; Masuzawa, T. Photolithography system with liquid crystal display as active gray-tone mask for 3D structuring of photoresist. *Sens. Actuators A Phys.* **2008**, *144*, 381–388.
[47] Njo, S. L.; van Asselt, R.; Broer, D. J.; de Witz, C. M. R. 23. 3: 23.3: Light-efficient liquid crystal displays using photoluminescent color filters. *SID Symp. Dig. Tech. Pap.* **2000**, *31*, 343–345.
[48] Ko, F. J.; Shieh, H. P. D. High-efficiency micro-optical color filter for liquid-crystal projection system applications. *Appl. Opt.* **2000**, *39*, 1159–1163.
[49] Wang, Y. Y.; Pan, J. A.; Wu, H. Q.; Talapin, D. V. Direct wavelength-selective optical and electron-beam lithography of functional inorganic nanomaterials. *ACS Nano* **2019**, *13*, 13917–13931.
[50] Wang, Y. Y.; Fedin, I.; Zhang, H.; Talapin, D. V. Direct optical lithography of functional inorganic nanomaterials. *Science* **2017**, *357*, 385–388.
[51] Hahm, D.; Park, J.; Jeong, I.; Rhee, S.; Lee, T.; Lee, C.; Chung, S.; Bae, W. K.; Lee, S. Surface engineered colloidal quantum dots for complete green process. *ACS Appl. Mater. Interfaces* **2020**, *12*, 10563–10570.
[52] Kang, H. L.; Kang, J. G.; Won, J. K.; Jung, S. M.; Kim, J.; Park, C. H.; Ju, B. K.; Kim, M. G.; Park, S. K. Spatial light patterning of full color quantum dot displays enabled by locally controlled surface tailoring. *Adv. Opt. Mater.* **2018**, *6*, 1701335.
[53] Ji, T. J.; Jin, S.; Zhang, H.; Chen, S. M.; Sun, X. W. Full color quantum dot light-emitting diodes patterned by photolithography technology. *J. Soc. Inf. Disp.* **2018**, *26*, 121–127.
[54] Müller, C. D.; Falcou, A.; Reckefuss, N.; Rojahn, M.; Wiederhirn, V.; Rudati, P.; Frohne, H.; Nuyken, O.; Becker, H.; Meerholz, K. Multi-colour organic light-emitting displays by solution processing. *Nature* **2003**, *421*, 829–833.
[55] Krotkus, S.; Ventsch, F.; Kasemann, D.; Zakhidov, A. A.; Hofmann, S.; Leo, K.; Gather, M. C. Photo-patterning of highly efficient state-of-the-art phosphorescent OLEDs using orthogonal hydrofluoroethers. *Adv. Opt. Mater.* **2014**, *2*, 1043–1048.
[56] Dong, Y. F.; Fang, Z. Q.; Look, D. C.; Doutt, D. R.; Cantwell, G.; Zhang, J.; Song, J. J.; Brillson, L. J. Defects at oxygen plasma cleaned ZnO polar surfaces. *J. Appl. Phys.* **2010**, *108*, 103718.
[57] Liu, L. S.; Mei, Z. X.; Tang, A. H.; Azarov, A.; Kuznetsov, A.; Xue, Q. K.; Du, X. L. Oxygen vacancies: The origin of n-type conductivity in ZnO. *Phys. Rev. B* **2016**, *93*, 235305.
[58] Lee, H. S.; Kim, D.; Han, J. H.; Lee, T. W.; Lee, S.; Jeon, D. Y.; Choi, K. C. Efficient quantum dot light-emitting diodes by reducing oxygen vacancies of ZnO nanoparticles with recycling process. *SID Symp. Dig. Tech. Pap.* **2019**, *50*, 1666–1668.
[59] Milleville, C. C.; Pelcher, K. E.; Sfeir, M. Y.; Banerjee, S.; Watson, D. F. Directional charge transfer mediated by mid-gap states: A transient absorption spectroscopy study of CdSe quantum dot/β-$Pb_{0.33}V_2O_5$ heterostructures. *J. Phys. Chem. C* **2016**, *120*, 5221–5232.
[60] Nagpal, P.; Klimov, V. I. Role of mid-gap states in charge transport and photoconductivity in semiconductor nanocrystal films. *Nat. Commun.* **2011**, *2*, 486.
[61] Bartnik, A. C.; Efros, A. L.; Koh, W. K.; Murray, C. B.; Wise, F. W. Electronic states and optical properties of PbSe nanorods and nanowires. *Phys. Rev. B* **2010**, *82*, 195313.